Article:
Lawes, M, Sharpe, GJ, Tripathi, N et al. (1 more author) (2016) Influence of spark ignition in the determination of Markstein lengths using spherically expanding flames. Fuel, 186. pp. 579-586. ISSN 0016-2361

https://doi.org/10.1016/j.fuel.2016.08.013

Influence of spark ignition in the determination of Markstein lengths using spherically expanding flames

M. Lawes[a], G.J. Sharpe[a], N. Tripathi[a,+], R.F. Cracknell[b,*]

[a] School of Mechanical Engineering, University of Leeds, Leeds, LS2 9JT, UK

[b] Shell Global Solutions, Brabazon House, Threapwood Road, Concord Business Park, Manchester, M22 0RR

[*] Corresponding author : Roger Cracknell

E-mail address :Roger.Cracknell@shell.com

Postal address : Shell Global Solutions, Brabazon House, Threapwood Road, Concord Business Park, Manchester, M22 0RR

Phone number : +161 499 4572

E-mail addresses of other authors

M. Lawes : M.Lawes@leeds.ac.uk

G.J. Sharpe : G.J.Sharpe@leeds.ac.uk

N Tripathi : Navanshu.Tripathi@shell.com

+ Now at Shell Global Solutions, Brabazon House, Threapwood Road, Concord Business Park, Manchester, M22 0RR

Type of article : full-length

Abstract

Constant pressure outwardly propagating flame experiments in a spherical bomb are performed to examine the duration and radius over which spark ignition effects persist. This is motivated by the need to properly account for such effects in the measurement of laminar burning velocity and Markstein length using the spark ignited expanding flame technique.

Ignition energy was varied and its effects on flame propagation in methane-air and isooctane-air mixtures were studied. The Markstein length of the mixture proved critical in the ignition energy dependency of flame propagation. For relatively high values, an underlying common variation of self-sustaining flame speed with radius can be identified by the rapid convergence of curves for different ignition energies. As the Markstein length decreases, low energy spark ignition is found to give rise to a distorted and wrinkled flame kernel. For such mixtures, due to the weak effect of stretch, the kernel subsequently develops into a non-spherically propagating flame. In these cases the spark ignition effect persists up to large radius. It is shown that using low ignition energy leads to a flame speed, during the development phase, which is higher than that of a self-sustaining spherical flame. It is further shown that if this effect is not accounted for, measurements of Markstein length using standard fitting techniques results in a large error. This problem is found to worsen as the Markstein length decreases, such that its apparent measured value becomes increasingly influenced by any distortions of the flame kernel produced by the spark.

Keywords : ignition; laminar; premixed; flame wrinkling; Markstein length

1. Introduction

The one-dimensional unstretched laminar burning velocity is a fundamental property of a combustible fuel-air mixture. It depends on the physico-chemical and chemical kinetic characteristics of the reactant mixture, which in turn are a function of the molecular structure of the fuel, as well as on the pressure and temperature. However, a major difficulty in its determination is that a planar and adiabatic flame rarely can be achieved. Most practical flames are three dimensional and do not conform to the idealized planar steady configuration. Instead they can be wrinkled, unsteady and can exist in flow fields that are themselves non uniform and unsteady. In such a situation, the laminar flame is stretched due to transverse velocity components and curvature. This necessitates the definition of another fundamental mixture parameter known as the Markstein length (defined below), which quantifies the

response of the flame to stretch rate. These two fundamental mixture parameters, the laminar burning velocity and Markstein length, are crucial validation tools in the development of chemistry and transport models and are necessary inputs for flamelet calculations, sub grid and turbulence models. Furthermore, knowledge of the laminar burning velocity, flame speed and effects of stretch rate are essential prerequisites to an understanding of turbulent flame development in engines and explosions.

The extrapolation of linear or non-linear relationships between flame stretch rate and flame speed to zero stretch values (see Section 2), has been extensively used to determine laminar burning velocity via outwardly propagating flame [1-5] and counter flow/stagnation flame measurements [6, 7]. However, care must be taken in identifying the regime of self-sustaining weakly stretched but spark unaffected flame, for which these relationships are valid [8-12]. In general, the inner limit of this regime at higher stretch rate is fixed by the decay of ignition effects, while the outer limit is determined by the combustion vessel size or the onset of instabilities at lower stretch rates. The choice of this range of data used for extrapolation is crucial for its accuracy and meaning [9-13]. Additionally, the selection of the outer limit should also ensure that the rise in pressure is small and the combustion vessel geometry does not start to influence flame propagation [14]. While the outer limit is readily identifiable, it is difficult to accurately pinpoint the inner limit at which the flame becomes independent of ignition effects and, therefore, its identification and quantification is a necessity.

Starting from the pioneering works of Zeldovich [15], several studies have aimed to understand the initiation and propagation of spherical flames. Some representative examples cited here address this issue either theoretically [16-20] or experimentally [21-25]. There has been increased understanding of several critical parameters (ignition energy, power, size of flame kernel), on the basis of which the criterion for successful flame ignition can be established [19]. Once a successful ignition has resulted in a developing flame kernel, its survival is controlled by the balance of the decreasing influence of the plasma, the increasing

contribution of combustion and the effects of flame stretch. This transition is gradual and it is difficult to delineate a stage, either spatially or temporally, when the spark influence has fully subsided and the contribution from combustion has fully developed [22]. Although some attempts have been made to study the influence of ignition in the early stages of flame development [20, 23, 25], they are concentrated towards measuring the critical radius for sustained flame propagation rather than addressing the issue of quantifying the limit of the spark affected zone. The limited studies which have discussed this issue, generally propose a fixed radius depending upon the experimental conditions, ignition hardware and the mixture [3-5, 19, 27-29].

In itself, ignition represents a classical phenomenon that is rich in fundamental processes of chemical kinetics (both low and high temperature kinetics) and fluid mechanics [30, 31]. Since flame ignition is inherently a transient process, fundamental studies dealing with ignition are directly relevant to other transient combustion phenomena such as flame stabilization, flammability limits and extinction, as well as to combustion efficiency and emissions [30]. Many technological applications focus specifically on flame initiation and transition to a developed state, for example, the interest of managing combustion in 'lean' reacting mixtures, particularly those approaching the flammability limits [32]. Furthermore, the continuing challenge in designing a more efficient and less polluting spark-ignited internal combustion engine leads to a desire to increase the consistency of the processes leading from spark ignition to fully developed flame. This also necessitates a better understanding of how a flame develops from an ignition source and the transition from an unreacted state to a fully developed burning state.

The present work aims to study the influence of ignition energy on the spatial and temporal development of flame speed, structure and the rate of stretch, and in particular to explore the scales over which ignition effects persist.

2. Experimental Apparatus and Methodology

A 380 mm diameter, spherical, stainless steel vessel was employed which was capable of withstanding the temperatures and pressures generated from explosions with initial pressures of up to 1.5 MPa and initial temperatures of up to 600 K [3]. It has extensive optical access through 3 pairs of orthogonal windows of 150 mm diameter and is equipped with four fans driven by electric motors. The fans were used to ensure that the reactants were well mixed and were stopped at least 2-3 minutes prior to ignition to ensure a quiescent mixture. The initial temperature and pressure in the present study were fixed for the entire set of experiments to 358 K and 0.3 MPa respectively. The study was conducted for methane-air and isooctane-air mixtures because of their strong and opposite non-equidiffusive behaviour for lean and rich flames. The initial temperature of 358 K was selected to ensure that the isooctane was completely vaporized before combustion at all equivalence ratios. For isooctane experiments, the volume of the fuel to be injected into the bomb was calculated from the required mole composition, the fuel density and the known volume of the bomb. Injection occurred with the air in the bomb at a pressure of about 0.005 MPa and measured partial pressures indicated when evaporation was complete. The pressure and temperature were measured immediately prior to ignition, which was initiated when the temperature was within 1K and the pressure was within 0.001 MPa of the intended value. There was no significant rise in chamber pressure during the period of flame observation; in the worst case the pressure rise was 0.01 MPa at a flame diameter close to the window size. In this case, the isentropic compression of the unburned gases resulted in a temperature rise of 3 K. Based upon [3]; this rise would lead to a negligible increase in the laminar burning velocity of about 0.8%.

Optical access allowed for imaging of the evolution of the centrally ignited expanding flame via a pin-hole schlieren system [33]. A high speed Phantom digital camera with 256 megabytes integral image memory was used at a camera speed of 4000 frames/s with 576*576 pixels and a resolution of 0.2655 mm/pixel.

Ignition was initiated by a trigger signal from the camera. An in-house manufactured ignition system was used. The system allowed current and discharge duration to be controlled separately [34]. The main spark unit was designed to discharge a capacitor, charged by a 600V DC power supply, through a spark gap of 1.25 mm. Control of the spark current was achieved with a bank of series resistors which could be isolated or included within the circuit through switches. Increasing the series resistance reduced the current through the spark gap. Steps of 0.1A and 0.5A were used for low energy setting which varied the current from 0 to 3A and steps of 0.75A was used for high energy setting which varied the current from 6A to 12A. The spark duration could be varied from 0 to 1 ms in steps of 10 μs. In the present study, current settings of 1, 3, 6 and 12 A and a fixed spark duration of 500 μs were employed. The voltage and current outputs were monitored by an oscilloscope for measuring the discharge energy. The duration of discharge (T) across the spark gap was obtained from the recorded pulse width. The discharged energy, E in mJ, across the spark gap is given by [35]

$$E = \int_0^T V(t) \times I(t) dt \qquad (1)$$

The ignition energies reported in the present work were calculated based upon breakdown currents and voltages measured in air under standard conditions (T=298K, P=0.1 MPa) and may not be identical to those in the methane and isooctane-air mixtures at given experimental conditions. The current settings of 1, 3, 6 and 12 A corresponded to energies being approximately 1, 16, 36 and 53 mJ respectively. This calculation intends only to estimate the relative magnitudes of energies at different current settings and is not a measure of the exact energy delivered to the flammable mixture. Furthermore, these energies represent the upper bound of ignition energy, as current and voltage might have been lost between the points of measurement and the electrodes.

Flame images were processed using an automated flame edge detection program for ease of processing and reduction of human bias. The initial pre-kernel image was subtracted from flame images to obtain an image of the flame solely, without spark plug. The subtracted flame images were binarised with white pixels representing the flame and black representing unburned gas. White pixels were counted and used to calculate flame area and mean flame radius (r), based on a spherical flame assumption. For each explosion, r was obtained from measurements of the projected flame area and was plotted against time. Flame speed (S_n), defined as dr/dt was found by numerical differentiation, using central differencing with a five point stencil in time. It should be noted that in the very early stages S_n is not a true flame speed but a propagation speed of the temperature front resulting from spark energy as well as chemical reaction.

Once the flame has progressed beyond the spark affected regime, changes in S_n arise partly from the decreasing proportion of unreacted mixture within the flame thickness and principally, from the changing total flame stretch rate (α) given by $(2/r) * S_n$ for a spherical flame [36]. Specifically, it is well established that stretch effects can be manifested through aerodynamic straining, flame curvature, and flame motion, and that these influences are particularly strong in the presence of mixture non-equidiffusion because of the resulting modification of the flame temperature [37]. However, the effects of unsteadiness can be neglected by limiting considerations to thin flames, having a large radius of curvature (with respect to the flame thickness) with slowly varying flame stretch rate (with respect to the flow transit time through the flame). For these conditions, in accordance with the Markstein theory [8] and its later generalization and extension [38], the relationship between S_n and α has been shown to be:

$$S_s - S_n = L_b \alpha \qquad (2)$$

Here L_b is the burned gas Markstein length for a given mixture, representing the sensitivity of flame speed to the stretch rate and S_s is the unstretched flame speed. Equation (1) can be represented by a plot of S_n against α, in which the extrapolating value of S_n at zero α is S_s and the negative of the gradient of the plot is represented by L_b. Since combustion is at constant pressure, the unstretched laminar burning velocity (u_l) is deduced using:

$$u_l = S_s(\rho_b/\rho_u) \tag{3}$$

in which ρ_b and ρ_u are the burned and unburned gas densities respectively.

3. Results

Shown in Figs. 1 to 4 are variations of flame speed with: (a) time; (b) radius and (c) rate of stretch for methane and air mixtures (Figs. 1 to 2) at ϕ = 1.4 and 0.8 and for isooctane and air mixtures (Figs. 3,4) at ϕ =0.8 and 1.4 respectively . Data is shown at T=353K and P=0.3Mpa for ignition energies of 11, 16, 36 and 53 MJ (unless the mixture failed to reliably ignite). Similar results for intermediate equivalence ratios, as well as expanded versions of figs 1-4 and are presented as supplementary material. Each curve in Figs. 1 to 4 represent the average from 3 explosions and the error bars represent the typical extent of their variation.

3.1 Early stages of flame development

Rich methane-air mixture results (ϕ =1.4) are presented in Fig. 1. The initial spark kernel radius increases with ignition energy and this is reflected in the increasing spatial location of minimum value of S_n with increasing energy. However, the temporal location of this minimum in Fig. 1(a), decreases slightly with increasing energy. Additionally the radius at which the flame exhibits the trends expected of a self-sustaining flame is a clear function of the ignition energy.

Lean methane-air mixtures (ϕ=0.8) are plotted for the full range of measurements in Fig. 2, In this case, the early stage evolution and development of S_n is quite different to that observed at ϕ=1.4 (Fig. 1). While S_n at the three higher ignition energies in Fig. 2 are initially (before about 2.5 ms, 6 mm) highly overdriven, for the lowest energy, S_n increases from an initially low value, before attaining a local maxima (at about 2 ms, 3 mm) and decreasing thereafter. The variation of the minimum values of S_n with ignition energy (annotated by point (1)) have the opposite trend to those at ϕ=1.4 in that the first local minimum value of S_n decreases with increasing ignition energy. While the curves for the three higher energies converge after about 4 ms and 9 mm, S_n at the lowest energy remains higher until about 7 ms and 13 mm. The symbols # and * and the gradient of the dashed line, L_b', shown on Fig. 2(c) are discussed in Section 3.2.

The above data for rich and lean methane-air mixtures represent mixtures with high and low Markstein lengths (L_b) respectively. An interesting comparison with these data is obtained by considering lean and rich isooctane-air mixtures in which the L_b trends are the opposite to those of methane. Figures 3 and 4 present the full range of data for lean (ϕ=0.8) and rich (ϕ=1.4) isooctane-air mixtures. The variation of S_n for the lean isooctane-air mixture, which has a high L_b, is quite similar to that for the rich methane-air which also has a high L_b. Also, the variation with ignition energy of the minimum in S_n and, its temporal and spatial locations have similar trends to the data in Fig. 1. The data in Fig. 3 show that, relative to the curve of S_n for the ignition energy of 11 mJ, the curves at 16, 36 and 53 mJ are initially, and progressively more, overdriven before all curves converge at larger times/radius and lower rates of stretch (in Fig. 3(c)). Data for isooctane-air at ϕ=1.4 is shown in Fig. 4. This mixture has a low L_b comparable to that of the lean methane air data in Fig. 2. Figure 4

shows similar trends to Fig. 2 in the variation of the minimum in S_n with ignition energy. However, unlike Fig. 2, the curves for all different energies in Fig. 4 remain distinct. Both in Figs. 2 and 4, one cannot readily identify a self-sustaining flame trajectory and hence it is difficult to obtain a time or radius beyond which the flame appears to be independent of ignition energy.

This behaviour wherein S_n at the lower energies remains greater than that for the higher energies for an extended zone was observed for isooctane-air mixtures at all $\phi \geq 1.1$ and for methane-air mixtures at $\phi = 0.8$. Reasons for this behaviour can be seen from observation of the schlieren images at ignition energies of 11 mJ and 53 mJ for isooctane-air flames in Figs. 5(a) to (d). Figure 5(a, b) correspond to $\phi = 0.8$ while (c, d) correspond to $\phi = 1.4$. All these images conform to approximately the same average radius of 8 mm and at times stated below the images. It is readily apparent that for $\phi = 0.8$ (Fig. 5(a, b), the flame is quite smooth. However for $\phi = 1.4$, the flame is significantly distorted with large-scale wrinkles or cracks at the lowest energy (Fig. 5(c)), while the flame at the highest energy (Fig. 5(d)) is relatively smoother and much closer to being spherical. Similarly, Fig. 6 (a) to (d) presents a comparison of schlieren images for methane-air flames at the extreme energies. Contrary to the data in Fig. 5, the flame for $\phi = 0.8$ at the lowest energy (Fig. 6(a)) appears most wrinkled and distorted. Flames for rich methane (Fig. 6(c, d)) are smoother and less distorted. Hence it appears that even though the spark creates a smooth flame kernel, in some cases it develops wrinkles on the surface at the lowest energy which persists up to large flame size. This wrinkling and distortion for the lowest energy in lean methane-air and rich isooctane-air mixtures, results in a greater flame surface area which leads to a higher average global S_n, consistent with Figs. 2 and 4. However, since the flame is not exactly spherical in Figs. 5(d) and 6(a), some caution is required in interpreting the S_n curves. It is re-iterated that the

average radius based upon the projected flame surface area has been used. Due to cracks and wrinkles, S_n and r will vary from point to point on the flame surface. For this reason, the speed of the flame surface position in different directions was also measured. While this indeed did vary with the direction chosen, the values were significantly higher than those of the more spherical high energy cases. The cause of development of these wrinkles at the lower energies is discussed in Section 4. The implications of using low ignition energy in the measurements of Markstein lengths are discussed below.

3.2 Effects of ignition energy in the determination of L_b and u_l

The novel finding described above of an increase in S_n for some mixtures following low energy ignition has important implications in measurements of S_s, u_l and L_b reported in the literature which have been determined from spherically expanding flames using the photographic technique. The technique for determining S_s and L_b requires fitting of flame speed variation against stretch rate to an expression such as Eq. (2) or one of its non-linear extensions [40]. While Eq. (2) may still be valid locally at a point on the flame surface, a global fit to low energy results, under the spherical assumption, may result in significant error in the accurate predictions of L_b and S_s. Here we attempt to quantify this error for cases where the flame is distorted following low energy ignition. Hereafter, a measured apparent value of L_b determined by assuming sphericity at a given energy will be denoted as L_b'. Hence, L_b is the fundamental burned gas Markstein length, which is intrinsic to a given mixture, while L_b' is the measured gradient determined by fitting to parts of the S_n against α data which appear linear in the S_n-α plane at a given energy. While higher order non-linear forms may also be used [5, 29], it is important to note that these also assume sphericity and, hence, will still result in similar errors in the fitting parameters.

We first quantify how the measured L_b' for low energy differs from L_b in the cases discussed above. This is important since in many previous works L_b' may have been assumed to represent the true L_b of the mixture.

The persistence of ignition effects is very marked for isooctane-air mixtures at ϕ=1.4. Figure 4(c) shows that the flame propagated differently at each of the four energies due to different extents of wrinkling at each energy, which was observed even for the highest energy. In this case, even before this ignition effect diminished, the flame already started to accelerate due to the onset of cellular instabilities. Bradley et al. [41] commented that for flames which become cellular very early, such as in lean hydrogen-air mixtures, and hence accelerate before any "self-sustaining" linear region develops, the concept of a laminar burning velocity is somewhat ill defined since such flames are always cellular in practice. However, the situation is even worse than this and the mixture limits for which global L_b and S_s measurements are meaningful concepts are confined to a narrow range of conditions. Even for mixtures where there may be a significant region in the S_n against α plane which apparently becomes linear before the fine scale wrinkling induced by cellularity causes a rapid acceleration e.g. shown in Fig. 4(c), the flame may still be strongly affected by ignition dependent distortions. For example, for mixtures such as rich isooctane-air at present experimental conditions, there is no region where the flame is free from ignition (non-spherical) effects or from instabilities. Hence, for such mixtures, measurement of L_b using standard techniques is unreliable and somewhat meaningless.

Similar dependence of L_b' on ignition energy is observed for lean methane-air mixture (ϕ=0.8) presented in Fig. 2(c). This is again a mixture which is weakly affected by α, and the differences in S_n against α trajectories for different energies persist throughout the flame propagation, up to the onset of cellularity. Although a roughly linear region of

propagation in the S_n against α plot can be determined for each energy individually, the slope of this linear region depends strongly on the energy. It is particularly interesting to note for this case that the sign of measured L_b' changes at the two extreme energies i.e. measured L_b' is close to 0.26 mm at 53 mJ while it is close to -0.11 mm at 11 mJ. Hence, once again the intrinsic L_b cannot be accurately determined for this case. However, the trends for mixtures with high positive L_b e.g. rich methane-air (ϕ=1.4) and lean isooctane-air (ϕ=0.8), as shown in Figs. 1(c) and 3(c) respectively, are quite contrasting. It is observed that S_n variation with α at different energies do collapse to roughly a common curve i.e. linearity in S_n against α plot is well established and easily identifiable. It is evident for such cases that measured L_b' is largely independent of the energy used and hence irrespective of energy, measured L_b' should be close to the true L_b of the mixture.

Figures 7 and 8 summarize the variation of L_b' against ignition energy for different ϕ of methane-air and isooctane-air mixtures respectively. Equivalent plots to figures 1-4 for intermediate equivalence ratio are given in the supplementary material from which the L_b' values are calculated The error bar in these figures is based upon the average of 3-4 explosions and takes into account the uncertainty of the choice of data range in which the S_n against α variation is somewhat subjectively taken to be linear. Some of the data points in Fig. 7 are plotted slightly offset from energy values of 16, 36 and 53 mJ to improve clarity by avoiding overlapping of error bars. For ϕ=1.1, 1.2 and 1.4, L_b' at a given ϕ is observed to be similar for all energies since the S_n against α curves converge on top of each other. However, for ϕ=1.0 and 0.8, L_b' differs across different energies, being highest for the highest energy. Moreover, these differences in L_b' become more pronounced as the mixture becomes leaner, with L_b' dropping more sharply at the lower energy end. For isooctane-air

mixtures in Fig. 8, similar values of L_b' were measured for ϕ=0.8 and 1.0. Similar to lean methane-air mixtures, differences in L_b' at different energies for a given ϕ, are observed for richer isooctane-air mixtures (ϕ=1.1, 1.2 and 1.4) as well and the ignition energy dependence of L_b' becomes more pronounced as we move richer.

Figures 7 and 8 reinforce the point that it is the mixtures which have negligible or negative dependence of S_n on α for which distortions in the flame kernel due to ignition effects can persist. In these cases stretch effects only slowly or insignificantly diminish any initial distortions introduced by the ignition. Conversely, for mixtures with high positive L_b, stretch rate rapidly washes out the initial distortions by pulling back the flame into a spherical shape. It should be noted that even in cases where L_b' measurements are strongly influenced by ignition energy, the measurements of S_s or u_l are almost independent of ignition energy. It is clear from Fig. 2(c) (and also S5 in the supplementary material) that even though the gradients of the linear regions differ with energy, interestingly S_n extrapolates to roughly similar S_s thereby yielding roughly a similar u_l.

4. Discussion

The principal motivation of this paper was to experimentally examine the point at which transient effects of spark ignition have subsided in order that these effects are minimized in the measurements of L_b and u_l. While variations in ignition energy may alter the rate of initiation, branching and propagation of chemical reactions [27, 42] for a given mixture and experimental conditions, the reactions driving the flame are essentially the same irrespective of the energy. Hence, once the chain reactions sustaining the flame are fully developed and the ignition influence has completely subsided, the burning rate as a function of flame stretch rate should be identical. For a spherically expanding flame, this implies that the convergence

of S_n trajectories at different energies indicate when ignition effects have subsided, the chemistry is fully developed and the flame has become self-sustaining.

Several previous papers give, or assume, a unique value of flame radius beyond which ignition effects can be neglected. This value is based upon a limited set of experiments and is even considered to be valid for different other mixtures and initial conditions [3-5, 18, 27-29]. Chen et al. [16] define a unique “critical radius" using numerical simulations based upon the point where the trajectories of two ignition energy curves converge in the S_n against α plot. However, it is clear from the above experimental results that while an optimum energy can in principle be identified for which the flame first becomes self-sustaining at the smallest radius, one cannot assign a unique or universal radius beyond which spark effects are not important, since the radius at which this occurs is in general strongly dependent on the energy itself. The higher the energy, the longer the flame remains overdriven and the larger the radius at which S_n approaches a self-sustaining curve. For example, critical radius in [20] will depend strongly on which two energies are used and the magnitude of the difference between them. Indeed, in principle this criterion could give an arbitrarily large radius if one of the energies is sufficiently high, even though the flame becomes independent of the spark much earlier using a small energy. Furthermore, even for the optimal energy at which the spark ignition effects diminish earliest, the radius at which this will occur is sensitive to the mixture and initial conditions and hence it is still not valid to assume a universal value. The results presented here indicate that for different mixtures and conditions it is important to perform experiments at several ignition energies if one truly wishes to determine a condition at which the spark effects can be neglected.

The above point is particularly salient for mixtures with low or negative L_b because of the novel finding reported here that due to persistent non-spherical effects produced by the ignition process itself, the S_n obtained using standard techniques may be significantly higher

than that of a spherically expanding flame. This was found to be particularly problematic at lower energies in these mixtures. Interestingly, several workers [2, 3, 43] employ ignition energy close to a minimum with the objective of minimizing spark disturbances during flame propagation and obtaining the quasi-steady self-sustaining curve at the earliest. Clearly, the above results show this to be incorrect for such mixtures. Bradley et al. [36] suggest a minimum energy might not be the best choice because the flame remains under driven for a long time. Conversely, we have shown that the apparent S_n appears overdriven for long time due to non-spherical ignition induced effects. Many authors [41, 43-45] have measured L_b for such mixtures using standard photographic techniques, without taking into account the errors introduced by ignition induced distortions and non-sphericity. An exception is Kelley et al. [25], who in their study on the measurement of critical radius for sustained flame propagation, recognized the theoretical requirement of maintaining a spherical ignition kernel. They optimized the spark gap and duration at each ϕ for attaining a spherical kernel. Again the above results suggest the need to perform experiments using several energies and also to examine the flame images to ensure that they are spherical, such that curve fitting of S_n as a function of α with assumed sphericity are valid, or to quantify the error if this is not the case. This becomes increasingly important as the L_b decreases. The above results show that one needs to be extremely cautious in determining L_b using standard spherically expanding flame techniques. For such low L_b mixtures, any inevitable cracks or distortions produced by the spark persist or are enhanced, and hence the flame does not propagate entirely spherically. These mixtures are also prone towards cellular instabilities because of the lack of positive stretch sensitivity. Hence, in these cases, regardless of ignition energy, the flame may be always subjected to either large-scale ignition induced or small scale intrinsic instability induced wrinkling and a spherical approximation never holds true at any stage of propagation.

Some previous studies [46, 47] also observed that wrinkles triggered by the spark, or electrode perturbations induced cracks over the flame front. These cracks did not branch to develop into cells and remained similar in morphology as the flame expanded. Under the assumption that absence of cell cracking to smaller scales did not affect the flame speed trajectory, [46, 47] concluded that the linear relationship between S_n and α is true and the extrapolation is valid. However, the present work presents evidence that even though the cells do not multiply, the degree of wrinkling on the flame surface, in itself depends upon the ignition energy. Hence, even though linearity between S_n and α holds, its gradient becomes increasingly dependent upon ignition energy as L_b decreases.

The question remains why the persistent large-scale distortion of the flame front becomes apparent for lowest energies. In spark ignition, ignition energy is discharged through the electrodes while the flame kernel develops around it. The contact of the flame kernel with the electrodes is inevitable and results in energy losses [16, 24, 48]. The initial kernel at lowest energy is in contact with the electrode surface for a considerable amount of time in comparison to that at the highest energy kernel. This prolonged contact, can act as a source of perturbation and deformity and also causes significant heat loss to the electrode surface, leading to a further weakening of the fragile flame kernel and increasing the propensity towards thermal diffusive instability driven distortion of the kernel [49, 50]. Localized disturbances arising from flame movement over the electrodes can persist and create cracks that propagate along the flame surface. When L_b is low, even after the flame has propagated away from ignition source, these disturbances persist for a longer period due to the local S_n variation being small, even though localized α may vary substantially. The heat losses are reduced for flame kernels following high energy ignition because it departs at an earlier stage from the region between the electrodes due to higher expansion velocity. Additionally, at higher ignition energies the flame kernel is more highly stretched, thereby reducing the

wrinkles and perturbations developing, if any. Therefore, higher ignition energy tends to give birth to a more stable and more spherical flame kernel, as observed by [28], but as L_b decreases, the stabilization by stretch becomes ineffective and hence the ignition effects persist longer.

5. Conclusions

In this paper, the effects of ignition energy on laminar expanding flames and the influence of this on the measurements of burning velocities and effects of stretch was investigated experimentally for methane-air and isooctane-air (representative of heavier hydrocarbon) mixtures. The main purpose was to examine how long spark ignition effects persist and hence determine the flame radius by which these effects have diminished and can be ignored when analyzing flame speed as a function of stretch rate. The main conclusions from the present study are summarized below.

1. The evolution and development of the flame kernel is strongly influenced by its response to flame stretch rate. For high Markstein length mixtures, flame speed against radius curves for different ignition energies converge rapidly, allowing identification of an underlying quasi-steady self-sustaining flame trajectory.
2. For lower Markstein length mixtures, ignition effects become more important. In these cases distortions in the emerging flame kernel produced by ignition can persist. These distortions are largest for lower energies since the struggling flame kernel remains near the electrodes longer. Hence the effects of these distortions are first seen at the lowest energy and manifests themselves as flame speed enhancement which persists up to large radius. As the Markstein length decreases, by changing equivalence ratio, and approaches zero or becomes negative, such initial flame kernel distortions become important even for higher energies. For very low Markstein length mixtures, it becomes difficult to find any region of self-sustaining spherical flame

propagation where either the ignition effects or the cellular instabilities are not present.

3. It is somewhat inappropriate to assign a unique or universal radius beyond which spark effects are not important, as the radius at which the flame approaches a spherical self-sustaining configuration is, in general, a function of the ignition energy together with the mixture and initial conditions.

Hence the main recommendations are that it is important to perform experiments with several ignition energies to determine conditions at which the flame is not affected by the spark for a given energy for different mixtures and initial conditions. This becomes increasingly important as the Markstein length decreases and, in particular, great care is needed to ensure measurement of Markstein length is a valid exercise for small or negative values. It is important to manually examine photographic records to ensure that the theoretical requirement of spherical flame is valid.

Acknowledgements

The authors are pleased to acknowledge the financial support of the Engineering and Physical Sciences Research Council (EPSRC) UK and Shell Global Solutions UK for N. Tripathi.

References

[1] D.R. Dowdy, D.B. Smith, S.C. Taylor, A. Williams, Proc. Combust. Inst. 23 (1990) 325–332.

[2] L.K. Tseng, M.A. Ismail, G.M. Faeth, Combust. Flame 95 (1993) 410-426.

[3] D. Bradley, R.A. Hicks, M. Lawes, C.G.W. Sheppard, R. Woolley, Combust. Flame 115 (1998) 126-144.

[4] X.J. Gu, M.Z. Haq, M. Lawes, R, Woolley, Combust. Flame 121 (2000) 41-58.

[5] A.P. Kelley, C.K. Law, Combust. Flame 156 (2009) 1844-1851.

[6] G. Jomaas, X.L. Zheng, D.L. Zhu, C.K. Law, Proc. Combust. Inst. 30 (2004) 193–200.

[7] K. Kumar, C.-J. Sung, Combust. Flame 151 (2007) 209–224.

[8] G.H. Markstein, Non-Steady Flame Propagation, Pergamon Press, New York, (1964).

[9] E. Varea, J. Beeckmann, H. Pitsch, Z. Chen, B. Renou, Proc. Combust. Inst. 35 (2015) 711–719

[10] J. Beeckmann, L. Cai, H. Pitsch, Fuel 117 (2014) 340–350

[11] H. H. Kim, S. H. Won, J. Santner, Z. Chen, Y. Ju, Proc. Combust. Inst. 34 (2013) 929–936

[12] O. Mannaa, M. S. Mansour, W. L. Roberts, S. H. Chung, Combust. Flame 162 (2015) 2311–2321

[13] Z. Chen, M.P. Burke, Y. Ju, Combust. Theory Modelling 13 (2009) 343-364.

[14] M.P. Burke, Z. Chen, Y. Ju, F.L. Dryer, Combust. Flame 156 (2009) 771-779.

[15] Y.B. Zeldovich, G.I. Barenblatt, V.B. Librovich and G.M. Makhviladze, The Mathematical Theory of Combustion and Explosions, Plenum Press, New York, (1985).

[16] R. Herweg, R.R. Maly, SAE Technical Paper Series 922243.

[17] T. Kravchik, E. Sher, J.B. Heywood, Combust. Sci. Technol. 108 (1995) 1-30.

[18] D. Bradley, P.H. Gaskell, X.J. Gu, Combust. Flame 104 (1996) 176-198.

[19] L. He, Combust. Theory Modelling 4 (2000) 159-172.

[20] Z. Chen, M.P. Burke, Y. Ju, Proc. Combust. Inst. 32 (2009) 1253-1260.

[21] G.T. Kalghatagi, Combust. Flame 60 (1985) 299-308.

[22] M. Champion, B. Deshaies, G. Joulin, K. Kinoshita, Combust. Flame 65 (1986) 319-337.

[23] Y. Ko, R.W. Anderson, V.S. Arpaci, Combust. Flame 83 (1991) 75-87.

[24] J. Song, D.H. Lee, Combust. Explos. Shock Waves 39 (2003) 513-524.

[25] A.P. Kelley, G. Jomaas, C.K. Law, Combust. Flame 156 (2009) 1006-1013.

[26] H. Willems, R. Sierens, J Eng Gas Turbines Power 125 (2003) 479–484.

[27] D. Bradley, F.K.K. Lung, Combust. Flame 69 (1987) 71-93.

[28] S.Y. Liao, D.M. Jiang, J. Gao, Z.H. Huang, Q. Cheng, Fuel 83 (2004) 1281-1288.

[29] F. Halter, T. Tahtouh, C. Mounaïm-Rousselle, Combust. Flame 157 (2010) 1825-1832.

[30] S.K. Aggarwal, Prog. Energy Combust. Sci. 24 (1998) 565-600.

[31] M.G. Andac, F.N. Egolfopoulus, Proc. Combust. Inst. 31 (2007) 1165-1172.

[32] A. Borghese, M. Diana, V. Moccia, R. Tamai, Combust. Sci. and Tech.. 1991. Vol. 76. pp. 219-231.

[33] J. Weinberg, Optics of Flames: Including Methods for the Study of Refractive Index Fields in Combustion and Aerodynamics, Butterworths, London (1963).

[34] F. K-K. Lung, Ph.D. Thesis, University of Leeds, Leeds, UK, (1986).

[35] C.C. Huang, S.S. Shy, C.C. Liu, Y.Y. Yan, Proc. Combust. Inst. 31 (2007) 1401-1409.

[36] D. Bradley, M. Lawes, M.S. Mansour, Combust. Flame 156 (2009) 1462-1470.

[37] C.K. Law, C.J. Sung, Prog. Energy Combust. Sci. 26 (2000) 459-505.

[38] P. Clavin, Prog. Energy Combust. Sci. 11 (1985) 1-59.

[39] N Tripathi, 'Dynamics of Confined Premixed Laminar Explosion Flames', Ph.D. Thesis, School of Mechanical Engineering, University of Leeds, 2012.

[40] P.D. Ronney, G.I. Sivashinsky, SIAM J. Appl. Math. 49 (4) (1989) 1029–1046.

[41] D. Bradley, M. Lawes, Kexin Liu, S. Verhelst, R. Woolley, Combust. Flame 149 (2007) 162–172.

[42] J.L. Beduneau, N. Kawahara, T. Nakayama, E. Tomita, Y. Ikeda, Combust. Flame 156 (2009) 642-656.

[43] S. Jerzembeck, N. Peters, P. Pepiot-Desjardins, H. Pitsch, Combust. Flame 156 (2009) 292–301.

[44] R.J. Johnston, J.T. Farrell, Proc. Combust. Inst. 30 (2005) 217–224.

[45] C. Mandilas, M.P. Ormsby, C.G.W. Sheppard, R. Woolley, Proc. Combust. Inst. 31 (2007) 1443-1450.

[46] G. Rozenchan, D.L. Zhu, C.K. Law, S.D. Tse, Proc. Combust. Inst. 29 (2002) 1461–1470.

[47] X. Wu, Z. Huang, X. Wang, C. Jin, C. Tang, L. Wei, C.K. Law, Combust. Flame 158 (2011) 539-546.

[48] G.T. Kalghatgi, Combust. Flame 77 (1989) 321-336.

[49] C.K. Law, Combustion Physics, Cambridge University Press, 2006.

[50] G. Joulin, P. Clavin, Combust. Flame (1979) 35:139–153.

Figure Captions

Figure 1 : Variation of S_n with (a) time; (b) radius and (c) stretch rate at different ignition energies. Methane-air mixture (ϕ=1.4, T=358 K, P=0.3 MPa).

Figure 2 : Variation of S_n with (a) time; (b) radius and (c) stretch rate at different ignition energies. Methane-air mixture (ϕ=0.8, T=358 K, P=0.3 MPa). The symbols # and * denote the start and end of the linear range used to obtain L_b' as discussed in Section 3.2.

Figure 3 : Variation of S_n with (a) time; (b) radius and (c) stretch rate at different ignition energies. Isooctane-air mixture (ϕ=0.8, T=358 K, P=0.3 MPa).

Figure 4 : Variation of S_n with (a) time; (b) radius and (c) stretch rate at different ignition energies. Isooctane-air mixture (ϕ=1.4, T=358 K, P=0.3 MPa).

Figure 5 : Comparison of flame structure at ignition energy of 11 and 53 mJ. Isooctane-air mixture (ϕ=0.8 and 1.4 at T=358 K and P=0.3 MPa).

Figure 6 : Comparison of flame structure at ignition energy of 11 and 53 mJ. Methane-air mixture (ϕ=0.8 and 1.4 at T=358 K and P=0.3 MPa).

Figure 7 : Variation of L_b' with ignition energy at different ϕ. Methane-air mixtures (T=358 K, P=0.3 MPa).

Figure 8 : Variation of L_b' with ignition energy at different ϕ. Isooctane-air mixtures (T=358 K, P=0.3 MPa).

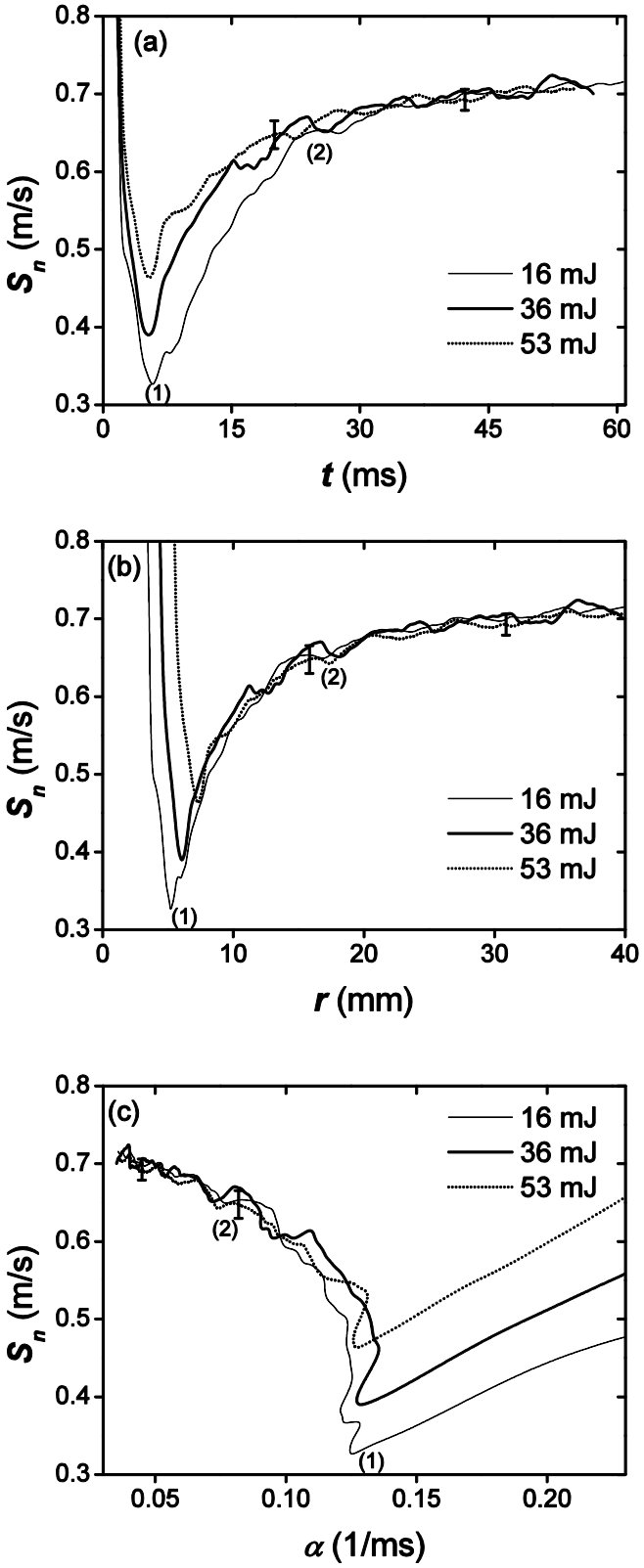

Figure 1 : Variation of S_n with (a) time; (b) radius and (c) stretch rate at different ignition energies. Methane-air mixture (ϕ=1.4, T=358 K, P=0.3 MPa).

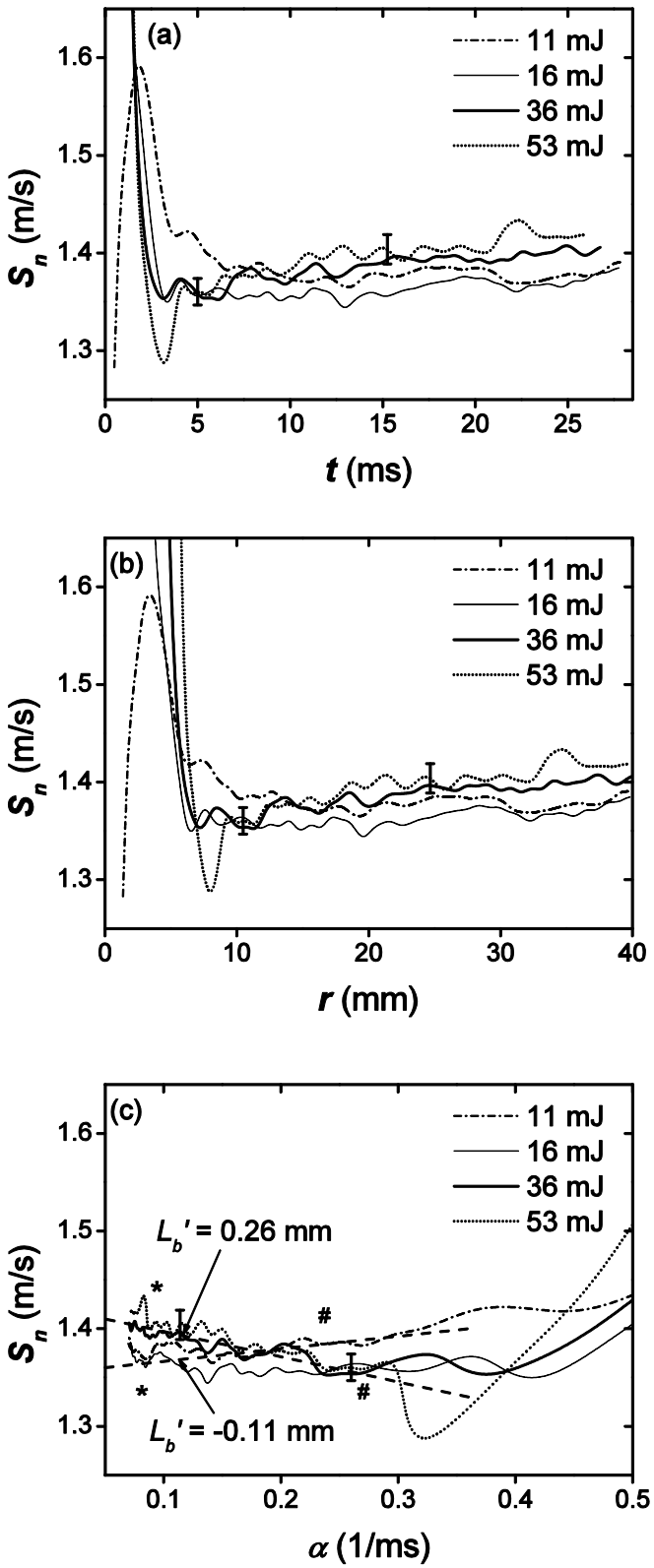

Figure 2 : Variation of S_n with (a) time; (b) radius and (c) stretch rate at different ignition energies. Methane-air mixture (ϕ=0.8, T=358 K, P=0.3 MPa). The symbols # and * denote the start and end of the linear range used to obtain L_b' as discussed in Section 3.2.

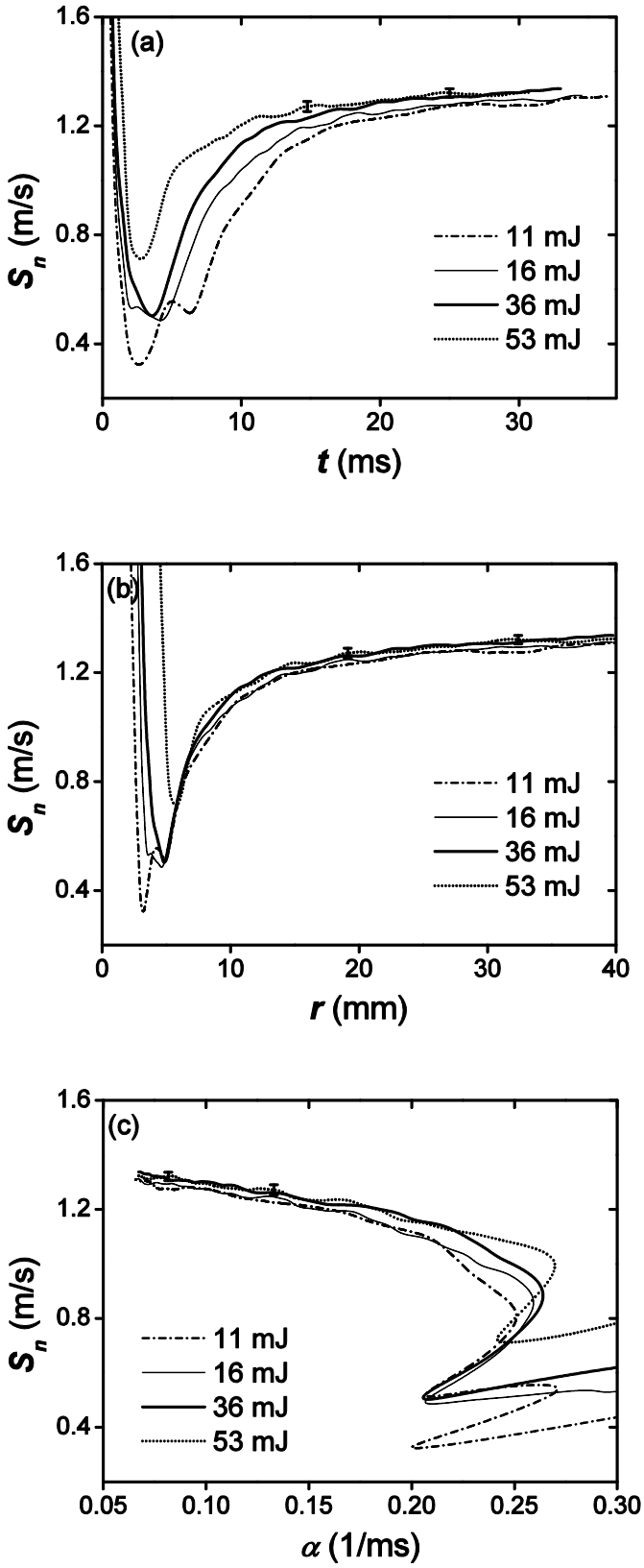

Figure 3 : Variation of S_n with (a) time; (b) radius and (c) stretch rate at different ignition energies. Isooctane-air mixture (ϕ=0.8, T=358 K, P=0.3 MPa).

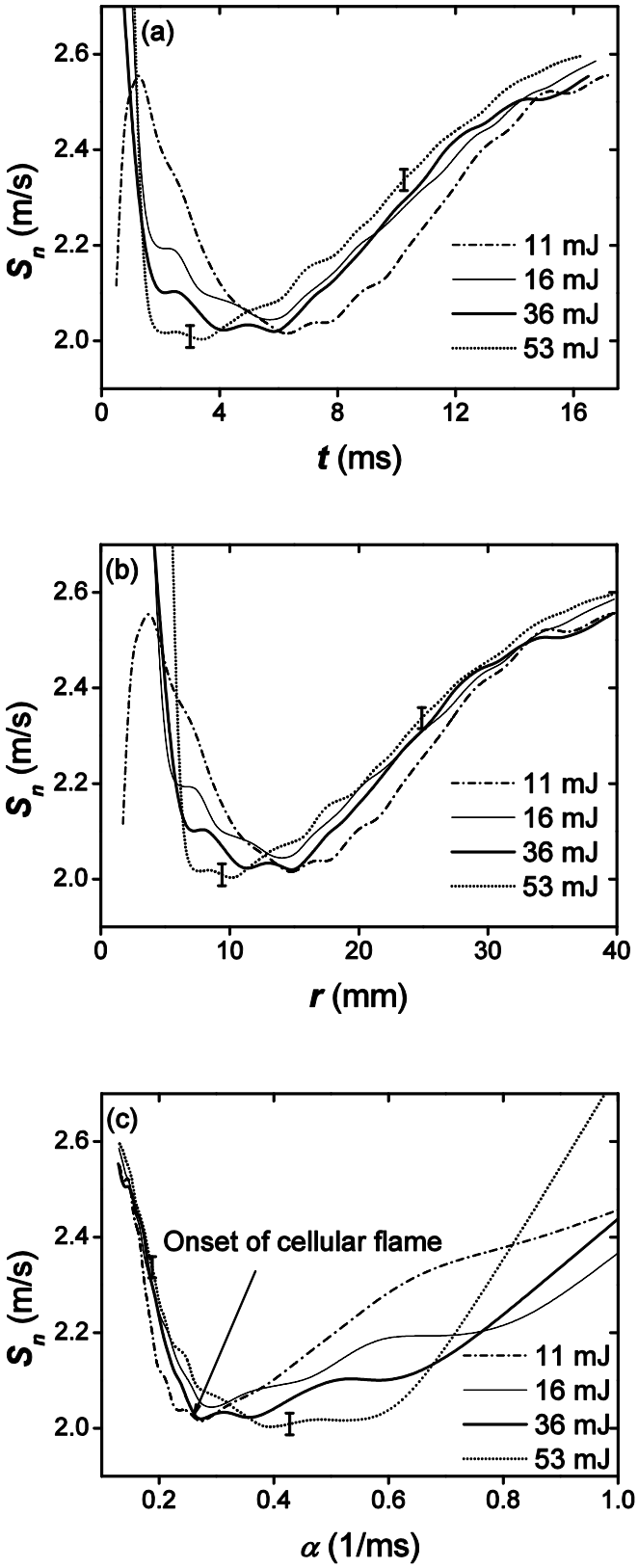

Figure 4 : Variation of S_n with (a) time; (b) radius and (c) stretch rate at different ignition energies. Isooctane-air mixture (ϕ=1.4, T=358 K, P=0.3 MPa).

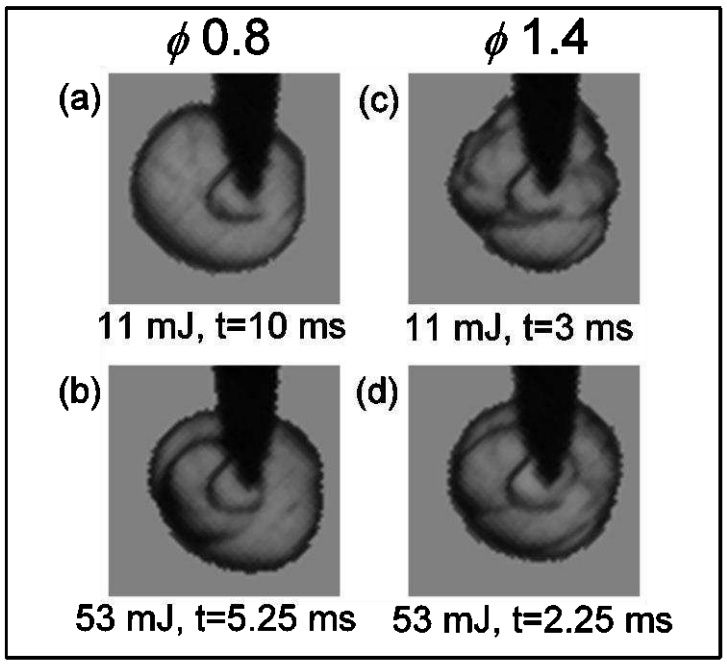

Figure 5 : Comparison of flame structure at ignition energy of 11 and 53 mJ. Isooctane-air mixture (ϕ=0.8 and 1.4 at T=358 K and P=0.3 MPa).

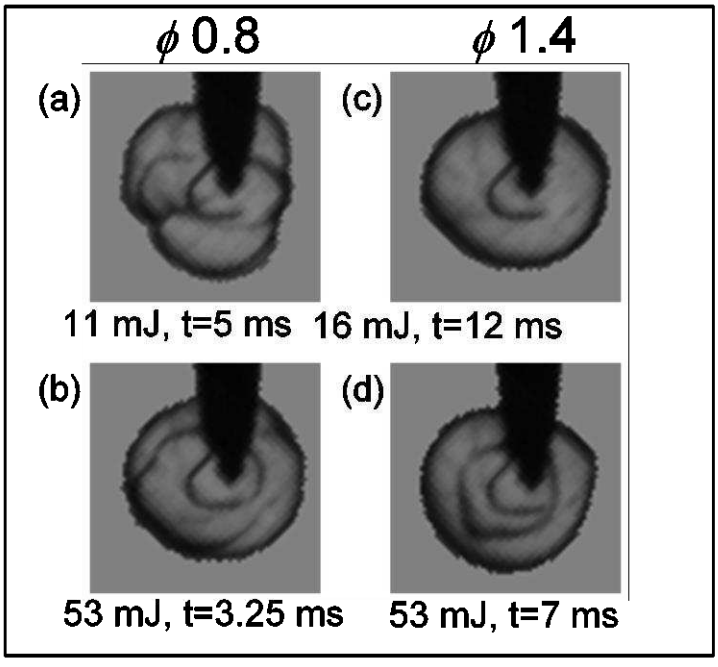

Figure 6 : Comparison of flame structure at ignition energy of 11 and 53 mJ. Methane-air mixture (ϕ=0.8 and 1.4 at T=358 K and P=0.3 MPa).

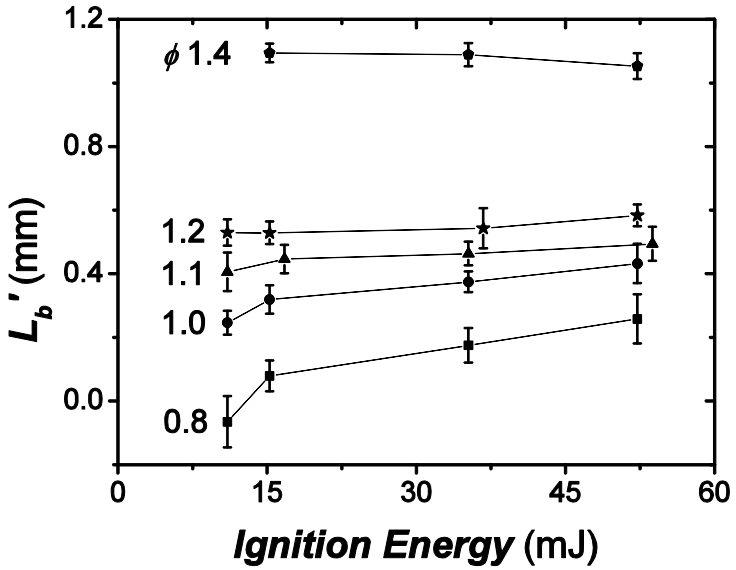

Figure 7 : Variation of L_b' with ignition energy at different ϕ. Methane-air mixtures (T=358 K, P=0.3 MPa).

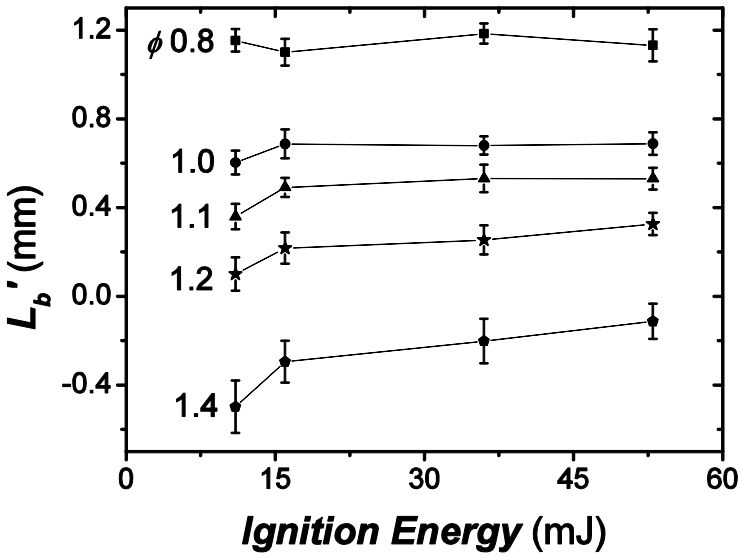

Figure 8 : Variation of L_b' with ignition energy at different ϕ. Isooctane-air mixtures (T=358 K, P=0.3 MPa).